

12-2016

Self-patterning Gd nano-fibers in Mg-Gd alloys

Yangxin Li
Shanghai Jiao Tong University

Jian Wang
University of Nebraska-Lincoln, jianwang@unl.edu


Kaiguo Chen
China Academy of Engineering Physics, Mianyang, Sichuan

Meiyue Shao
Shanghai Jiao Tong University

Yao Shen
Shanghai Jiao Tong University, yaoshen@sjtu.edu.cn

See next page for additional authors

Follow this and additional works at: <http://digitalcommons.unl.edu/mechengfacpub>

 Part of the [Mechanics of Materials Commons](#), [Nanoscience and Nanotechnology Commons](#), [Other Engineering Science and Materials Commons](#), and the [Other Mechanical Engineering Commons](#)

Li, Yangxin; Wang, Jian; Chen, Kaiguo; Shao, Meiyue; Shen, Yao; Jin, Li; and Zhu, Guo-zhen, "Self-patterning Gd nano-fibers in Mg-Gd alloys" (2016). *Mechanical & Materials Engineering Faculty Publications*. 199.
<http://digitalcommons.unl.edu/mechengfacpub/199>


This Article is brought to you for free and open access by the Mechanical & Materials Engineering, Department of at DigitalCommons@University of Nebraska - Lincoln. It has been accepted for inclusion in Mechanical & Materials Engineering Faculty Publications by an authorized administrator of DigitalCommons@University of Nebraska - Lincoln.

Authors

Yangxin Li, Jian Wang, Kaiguo Chen, Meiyue Shao, Yao Shen, Li Jin, and Guo-zhen Zhu

This work is licensed under a Creative Commons Attribution 4.0 International License.

SCIENTIFIC REPORTS



OPEN

Self-patterning Gd nano-fibers in Mg-Gd alloys

Yangxin Li^{1,2}, Jian Wang³, Kaiguo Chen⁴, Meiyue Shao², Yao Shen¹, Li Jin² & Guo-zhen Zhu¹

Received: 27 July 2016
 Accepted: 10 November 2016
 Published: 07 December 2016

Manipulating the shape and distribution of strengthening units, e.g. particles, fibers, and precipitates, in a bulk metal, has been a widely applied strategy of tailoring their mechanical properties. Here, we report self-assembled patterns of Gd nano-fibers in Mg-Gd alloys for the purpose of improving their strength and deformability. 1-nm Gd nano-fibers, with a $\langle c \rangle$ -rod shape, are formed and hexagonally patterned in association with Gd segregations along dislocations that nucleated during hot extrusion. Such Gd-fiber patterns are able to regulate the relative activities of slips and twinning, as a result, overcome the inherent limitations in strength and ductility of Mg alloys. This nano-fiber patterning approach could be an effective method to engineer hexagonal metals.

Microstructure engineering is a persistently vigorous technique in altering material's properties through tailoring geometrical features of structural units at multiple length scales and modifying three-dimensional arrangements of structural units. Structural units can be classified into three, two, one, or zero dimensions, such as three-dimensional volumes^{1,2} (phases, grains, particles/precipitates), two-dimensional surfaces^{3,4} (boundaries, interphases), one-dimensional lines (triple lines, edges, dislocations) or zero-dimensional points (quadruple points, vertices on polyhedral particles)⁵. In advancing the material's performance resulted from these structural units, arranging their distribution provides different strategies in addition to regulating the dimensions and shapes of these structural units. To realize specific microstructure, heat treatment, mechanical deformation, and/or their combinations can be applied while adjusting chemical compositions of a material.

Rare-earth (RE) elements⁶ has a demonstrated significance in tuning the microstructure of Mg alloys, such as weakening basal texture of Mg alloys^{7,8}, refining grain sizes, forming long-period stacking-ordered structure⁴, etc. RE solutes can also be trapped in twin boundaries, and in turn, impeding migration of twin boundaries^{9,10}. In addition, the elastic interactions between solutes and dislocations lead to solute segregation and depletion around dislocation cores. Such a solute atmosphere, which can maintain their confined structural and chemical states over a range of evaluated temperatures¹¹, produces a drag force on the moving dislocations, pins the dislocation motion, and thus modifies the mechanical performance of materials.

Here, we reported self-assembled hexagonal patterns of Gd-segregated dislocations that have a $\langle c \rangle$ -rod shape. These pinned dislocations act as the predictable inhibitor for basal slips because the glide of basal dislocations must cut them, but less affect the glide of non-basal prismatic dislocations because they are on the parallel planes. Additionally, the crystal domains, strengthened by such pinned dislocation patterns, can effectively impede twin propagation. As a result, such dislocation patterns can change the relative mobility of plastic deformation carriers (dislocations and twins).

Methods

Mg-1Gd (wt.%) alloy billets were prepared through melting high purity Mg (99.99%) and Mg-25 wt.%Gd master alloys in an electric furnace under a protective gas mixture of SF₆/CO₂. The billets were partly indirect extruded, at temperatures of 400 °C with extrusion ratio of 16, up to 150 mm from the die. After that, the die and butt were removed from the machine and quenched together into a water bath. Samples then were isochronally annealed at 200 °C, 250 °C, 300 °C for 2–4 hours. TEM samples were prepared through twin-jet electro-polishing methods and additional ion polishing at 500 eV for 0.5 h using Gatan precision ion polishing system (PIPS II MODEL 695). Structural characterization was carried out under scanning transmission electron microscopy (STEM) mode at

¹State Key Laboratory of Metal Matrix Composites, Shanghai Jiao Tong University, 800 Dongchuan Rd., Shanghai, 200240, P.R. China. ²National Engineering Research Center of Light Alloy Net Forming, School of Materials Science and Engineering, Shanghai Jiao Tong University, 800 Dongchuan Rd., Shanghai, 200240, P.R. China. ³Department of Mechanical and Materials Engineering, University of Nebraska-Lincoln, Lincoln, NE, 68588, USA. ⁴National Key Lab of Shockwave and Detonation Physics, Institute of Fluid Physics, China Academy of Engineering Physics, Mianyang, Sichuan, 621000, P.R. China. Correspondence and requests for materials should be addressed to Y.S. (email: yaoshen@sjtu.edu.cn) or L.J. (email: j_jinli@sjtu.edu.cn) or G.-z. Z. (email: zhugz@sjtu.edu.cn)

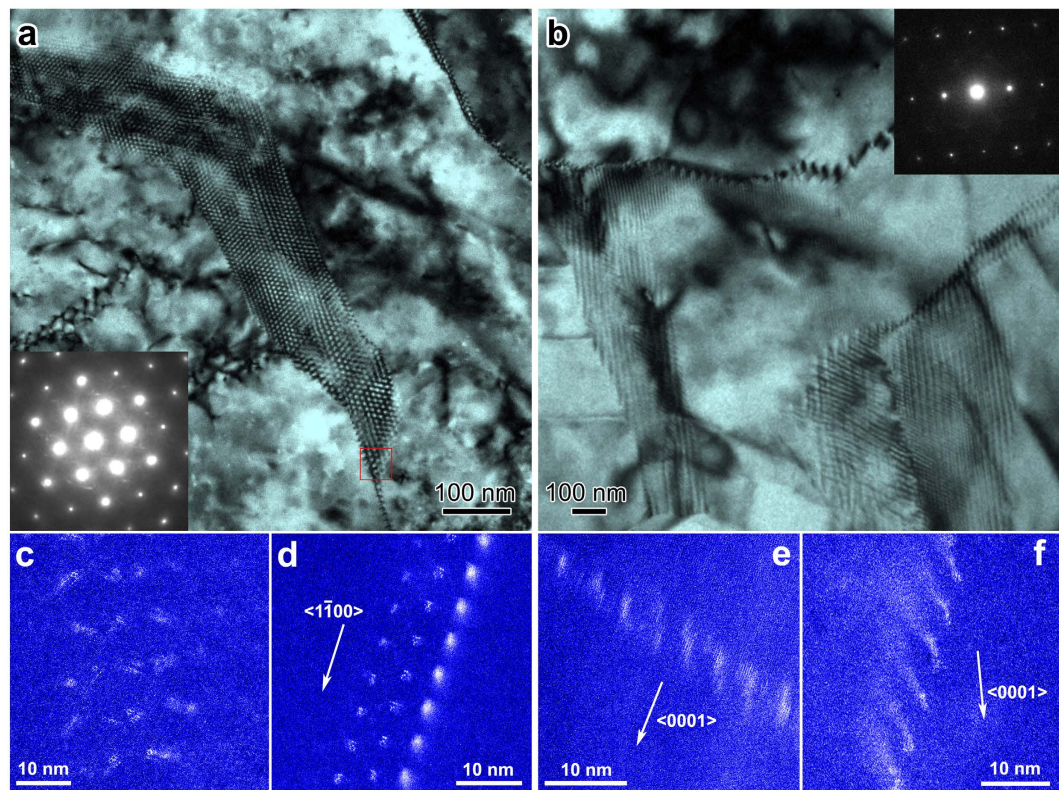


Figure 1. Gd nano-fiber patterns. (a and b) are Transmission Electron Microscopy Bright-Field (TEM-BF) images of the typical Gd segregation patterns within binary Mg-Gd alloys, viewed from $\langle 0001 \rangle$ and $\langle 1\bar{1}00 \rangle$, respectively. (c–f) scanning TEM High-Angle Annular Dark-Field (STEM-HAADF) images showing Gd segregation in the bright contrast. Panel c is the enlarged view of boxed region in (a). (d) is a different Gd nano-fiber pattern viewed from $\langle 0001 \rangle$. The beam direction for (e and f) is $\langle 1\bar{1}00 \rangle$.

200 kV using a JEOL-ARM200F microscope with a probe-forming lens corrector. Due to the large difference in atomic numbers of Gd and Mg, high-angle annular dark-field (HAADF) imaging technique was applied to image Gd atoms in binary Mg-Gd alloys.

Results

Within binary Mg-Gd alloys after hot extrusion at 400 °C, we for the first time observed hexagonally patterned domains, which have a width of less than 200 nm and several microns in length, dispersive in the Mg matrix. Viewed from the $\langle c \rangle$ -axis in Fig. 1a (more details in Fig. S1), each hexagonal pattern has an identical interspacing, which varies from 5 nm to 20 nm. Most domains have an interspacing of ~ 10 nm. The hexagonal patterns consist of Gd segregated clusters, shown as the bright intensity in the Z-contrast images (scanning transmission electron microscopy-high-angle annular dark-field, STEM-HAADF images) in Fig. 1c–f. The Gd segregations can slightly deviate from ideal hexagonal positions (see Fig. 1c,d). Viewed from the $\langle b \rangle$ -axis ($\langle 1\bar{1}00 \rangle$) in Fig. 1b, straight-line features associated with the patterned fibers are characterized with interspacings of 5–15 nm. These straight-line features, lying along the $\langle c \rangle$ -axis, turn out as Gd-rich fibers with ~ 1 nm in diameter. (Fig. 1e,f and Fig. S4). Combining the two orthogonal projections, we believe that Gd nano-fibers with the $\langle c \rangle$ -rod shape are self-assembled into hexagonal patterns within the Mg matrix.

These directional nano-rods cannot exist without the dislocation module because the capillarity effect prevents them from forming at the nanoscale. Further crystallographic analysis reveals that these Gd nano-fibers are Gd-segregated dislocations. Some of these dislocations are characterized with the Burgers vector $1/3 \langle 11\bar{2}0 \rangle$ that is identified using the Burgers circuit method (see Fig. 2e–h). It is worth mentioning that short-range orders of Gd atoms, such as hexagonal rings and zigzag patterns, were recorded in more than 70% of the Gd segregations (see Figs 1c,d and 2). These characteristics of Gd short-range orders agree well with the observation in experiments and simulations^{12,13}. The Gd rings always present at the dilated part of the dislocations because Gd has $\sim 20\%$ larger radius than Mg. The hexagonal patterns contain a set of Gd-segregated $1/3 \langle 11\bar{2}0 \rangle$ dislocations, which have the Burgers vectors either parallel or with 60° rotation, as shown in Fig. 2e,f. Some Gd-segregated dislocations may have Burgers vectors of $\langle 0001 \rangle$, because Burgers circuits are closed for such dislocations after we analyzed more than 20 hexagonal patterns (See those in Fig. 2f). The $\langle c \rangle$ -screw character of these dislocations can be additionally supported by a large number of dislocations with $\langle c \rangle$ -components through the Burgers vector analysis under two-beam conditions (See Fig. S3). These distinctive dislocations cause a few degrees misorientation between the adjacent grains bonded by one hexagonal pattern, as evidenced by sharp adjacent spots from the Fast Fourier Transform (FFT) of the hexagonal patterns (see insets in Fig. 2a,b and d).

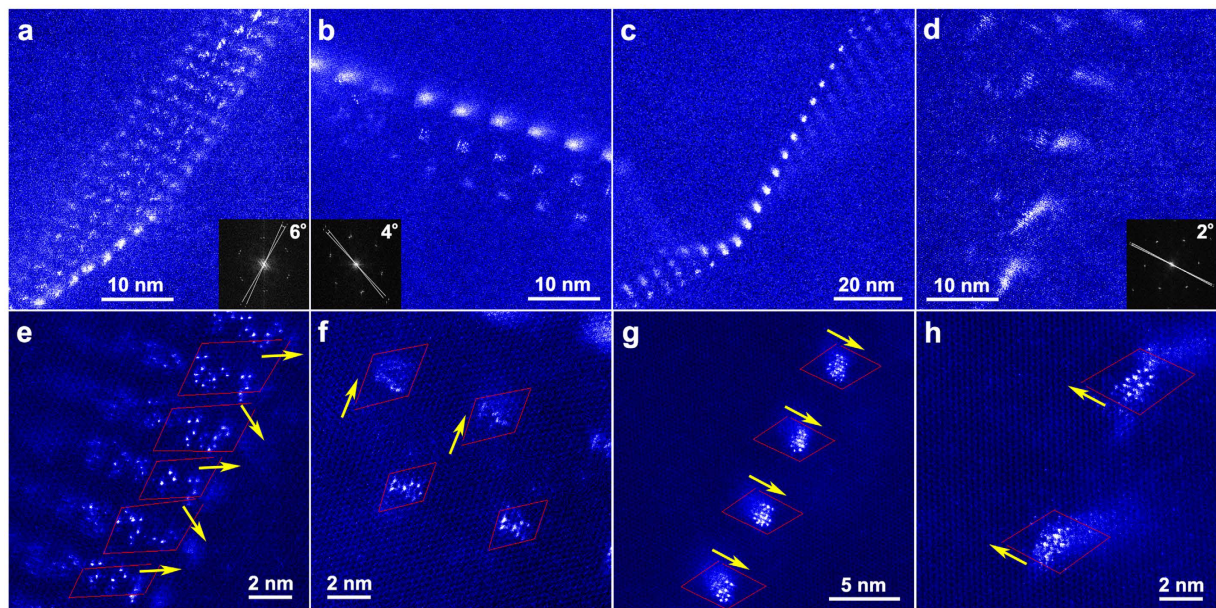


Figure 2. STEM-HAADF raw images of annealed samples. From left to right, Gd nano-fibers have an interspacing of ~ 3 nm, ~ 6 nm, and ~ 10 nm, in corresponding to a measurable rotation angle of 6° , 4° , and 2° between the adjacent lattices. Insets in (a, b and d) are the corresponding Fast Fourier Transform (FFT) images. (e–h) are enlarged view of regions selected from (a–d), respectively. The identified Burgers vectors, along crystallographic directions of $1/3 \langle 11\bar{2}0 \rangle$, are labeled by yellow arrows. The Gd hexagonal rings and zigzag patterns within the dislocation cores are clearly recorded.

The Gd nano-fiber hexagonal patterns are commonly observed near low-angle grain boundaries, which also consist of Gd-segregated dislocations (see details in Figs 1 and 2 and Fig. S2). A huge number of low-angle grain boundaries are randomly distributed within deformed grains with a few microns in size. The average spacing of Gd-segregated dislocations within the low-angle grain boundaries is around 3–15 nm, corresponding to the measurable misorientation angles of 1 – 6° about the $\langle c \rangle$ -axis. This is in agreement with the analysis according to Frank's law¹⁴. A significant Z-contrast of Gd nano-fiber patterns was detected when the interspacing of Gd-segregated dislocations is ~ 3 – 10 nm (see Fig. 2a–d). Gd-segregated dislocations are barely visible and irregularly patterned in a hexagonal shape as increasing the interspacing, e.g. 20 nm (see Fig. S5).

Discussion

Hexagonal patterns of Gd nano-fibers discovered in binary Mg–Gd alloys are dependent on annealing temperature. Before extrusion, Gd nano-fiber patterns were not detected in as-cast samples. The as-extruded microstructure was frozen by the indirect extrusion method, in which the die and butt were modified with fast quenching capability. Using TEM-BF techniques, we detected the same hexagonal patterns in as-extruded samples (Fig. S1) as in the annealed samples at 200°C we showed before. The difference is that the as-extruded Gd segregation spreads in a “near-honeycomb” pattern (Fig. 3) or other irregular pattern (Fig. S6) with ~ 10 nm in diameter, compared to the two-dimensional arrays of Gd nano-fibers. An array of $1/3 \langle 11\bar{2}0 \rangle$ dislocations was observed with nearly random Gd solutes around their cores (Fig. 3b). These messy arrays further evolve into the perfect hexagonal pattern consisting of 1-nm Gd fibers after 200°C and 250°C annealing for 2–4 hours. We did not find any hexagonal pattern or 1-nm Gd fibers within the sample after 300°C annealing (Fig. S7). The disappearance of such hexagonal pattern is possibly ascribed to recrystallization¹⁵. Thus, 1-nm Gd fibers and the corresponding hexagonal patterns would be favorably formed after moderate temperature annealing, (e.g. 200 – 250°C) while destroyed at elevated temperatures.

The puzzle of patterning Gd fibers in a hexagonal shape can be understood in the framework of dislocation interaction. Corresponding to characteristics of dislocation patterns in Fig. 2, we assumed that a hexagonal pattern is comprised of $\langle c \rangle$ screw dislocations with alternative signs and an array of $\langle c+a \rangle$ dislocations, as shown in Fig. 4. This model was proposed based on the facts: (a) no extra misorientation was detected between the adjacent grains across the hexagonal pattern except the one caused by the low-angle grain boundary (represented by an array of $\langle c+a \rangle$ dislocations); (b) the FFT of the local area is very sharp indicating a sharp, rather than a gradual transition of orientations; (c) there is no elastic interactions between $\langle c \rangle$ screw dislocations and $\langle a \rangle$ edge dislocations because they are perpendicular to each other. We found that the maximum resolved stresses on individual slip systems are estimated to be smaller than $4 \times 10^{-3} \mu$ for the $\langle c \rangle$ screw dislocations inside the pattern as the interspacing is 10 nm. Where μ is shear modulus. Thus, the formation can be rationalized as follows. Once a low-angle grain boundary formed by the spatial pileup of $\langle c+a \rangle$ prismatic dislocations, $\langle c \rangle$ dislocations can come from two sources, either activated $\langle c \rangle$ slips or the resultant of $\langle c+a \rangle$ dislocations that are repelled by the grain boundary and react to each other and form $\langle c \rangle$ dislocations. These dislocations are then self-assembled in

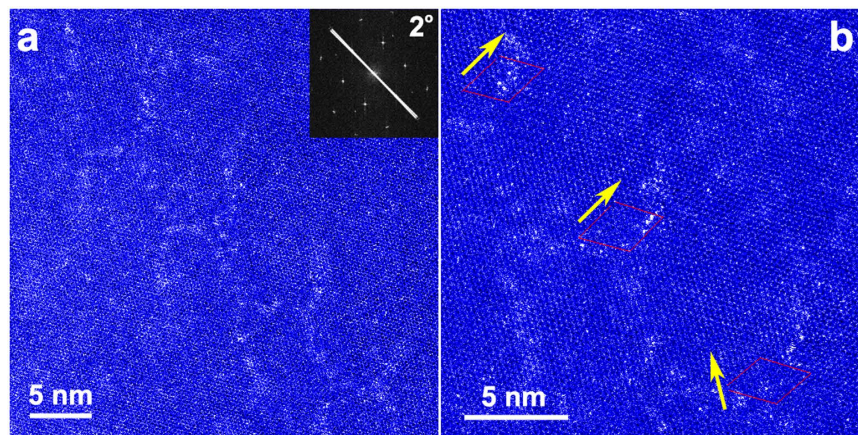


Figure 3. STEM-HAADF raw images of the as-extruded sample. The inset FFT graph in (a) shows that the adjacent lattices have a rotation angle of 2° . (b) enlarged view of the same region in (a). Gd atoms, as bright dots in the HAADF images, has no clearly pattern but preferentially located near the defected regions. The identified components of Burgers vectors $1/3\langle 11\bar{2}0 \rangle$ are labeled as yellow arrows.

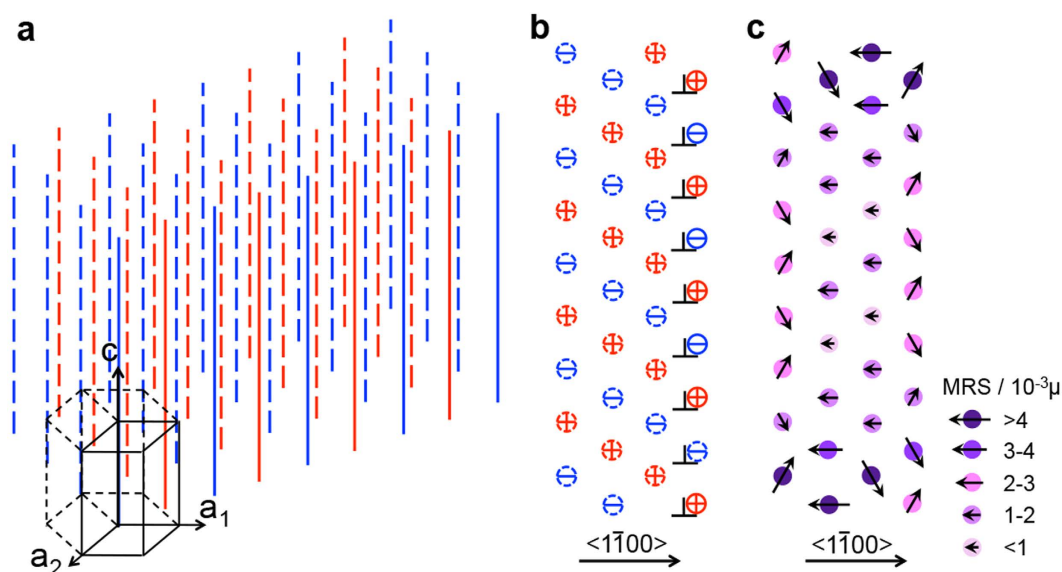


Figure 4. Schematics of the dislocations pattern. (a) 3D dislocation structure. The low-angle grain boundary is represented by an array of mixed $\langle c+a \rangle$ dislocations. $\langle c \rangle$ screw dislocations are represented in dashed lines, positive in red and negative in blue. The mixed dislocations are represented in solid lines, positive in red and negative in blue. Panel b shows the dislocations pattern viewed along $\langle 0001 \rangle$, and (c) is the distribution of maximum resolved stresses (MRS) on each dislocation.

a hexagonal pattern due to the elastic interaction. Such patterns could be stabilized by the Peiers stress of the $\langle c \rangle$ screw dislocation, which is greater than the maximum resolved stresses^{16,17}.

From mechanical viewpoint, the pinned dislocations in the pattern could inhibit the easy basal slips by the “forest” strengthening mechanism¹⁸, for the purpose of strengthening Mg alloys, while crystal domains strengthened by such pinned dislocation patterns can effectively impede twin propagation, in turn, reducing twinning while improving deformability of Mg alloys. The tensile tests for normally extruded samples (containing no Gd-fiber pattern) and indirect-extruded samples (containing the embryo of Gd-fiber patterns) indicate that the self-patterning Gd nano-fibers do improve the mechanical responses (Fig. S9). Thus, introducing patterned Gd nano-fibers might provide a new path for manufacturing advanced hexagonal alloys in general.

References

1. Park, J. M. *et al.* Microstructural modulations enhance the mechanical properties in Al-Cu-(Si, Ga) ultrafine composites. *Adv. Eng. Mater.* **12**, 1137–1141 (2010).
2. StJohn, D. H. *et al.* Grain refinement of magnesium alloys. *Metall. Mater. Trans. A* **36**, 1669–1679 (2005).
3. Zhang, W. Z. & Weatherly, G. C. On the crystallography of precipitation. *Prog. Mater. Sci.* **50**, 181–292 (2005).

4. Nie, J. F. Precipitation and hardening in magnesium alloys. *Metall. Mater. Trans. A* **43**, 3891–3939 (2012).
5. Tamirisakandala, S. & Miracle, D. B. Microstructure engineering of titanium alloys via small boron additions. *Int. J. Adv. Eng. Sci. Appl. Math.* **2**, 168–180 (2010).
6. Rokhlin, L. L. *Magnesium Alloys Containing Rare Earth Metals*. (Taylor and Francis, London, U.K., 2003).
7. Stanford, N. *et al.* Effect of microalloying with rare-earth elements on the texture of extruded magnesium-based alloys. *Scripta Mater.* **59**, 772–775 (2008).
8. Wu, W. X. *et al.* Grain growth and texture evolution during annealing in an indirect-extruded Mg-1Gd alloy. *J. Alloy. Compd.* **585**, 111–119 (2014).
9. Nie, J.-F. *et al.* Periodic segregation of solute atoms in fully coherent twin boundaries. *Science*, **340**, 957–960 (2013).
10. Kumar, A., Wang, J. & Tomé, C. N. First-principles study of energy and atomic solubility of twinning-associated boundaries in hexagonal metals. *Acta Mater.* **85**, 144–154 (2015).
11. Kuzmina, M. *et al.* Linear complexions: confined chemical and structural states at dislocations. *Science* **349**, 1080–1083 (2015).
12. Nishijima, M. & Hiraga, K. Structural changes of precipitates in an Mg-5 at% Gd alloy studied by transmission electron microscopy. *Mater. Trans.* **48**, 10–15 (2007).
13. Kimizuka, H. & Ogata, S. Predicting atomic arrangement of solute clusters in dilute Mg alloys. *Mater. Res. Lett.* **1**, 213–219 (2013).
14. Frank, F. C. & van der Merve, J. H. One-dimensional dislocations. I. Static theory. *Proc. R. Soc. A* **198**, 205–216 (1949).
15. Zhang, X. P. *et al.* Microstructure; bonding strength and thickness ratio of Al/Mg/Al alloy laminated composites prepared by hot rolling. *Mater. Sci. Eng. A.* **528**, 1954–1960 (2011).
16. Tasi, J. A. *et al.* First-principles data for solid-solution strengthening of magnesium: From geometry and chemistry to properties. *Acta Mater.* **58**, 5704–5713 (2010).
17. Leyson, G. P. M. *et al.* Quantitative prediction of solute strengthening in aluminum alloys. *Nature Mater.* **9**, 750–755 (2010).
18. Madec, R. *et al.* From dislocation junction to forest hardening. *Phys. Rev. Lett.* **89**, 255508 (2002).

Acknowledgements

We acknowledge funding from 1000Plan Professorship for Young Talents Program, the National Natural Science Foundation of China (Nos 51401124, 51471107, 51271118, 51671132). J.W. thanks the support by the Nebraska Center for Energy Sciences Research and acknowledges research sponsorship by DOE, Office of Basic Energy sciences. K.C. acknowledges the CCS Project Grant No. YK2015-0202002. We thank Prof. John Hirth for his valuable comments on our manuscripts.

Author Contributions

G.-z. Z., J. W. and Y. S. wrote the manuscript. M.Y. S. and L. J. were responsible for the alloy preparation, Y.X. L. and G.-z. Z. for TEM experiments, Y. S. and K. C. for dislocation simulation. All authors discussed the results and contributed to the improvement of the manuscript text.

Additional Information

Supplementary information accompanies this paper at <http://www.nature.com/srep>

Competing financial interests: The authors declare no competing financial interests.

How to cite this article: Li, Y. *et al.* Self-patterning Gd nano-fibers in Mg-Gd alloys. *Sci. Rep.* **6**, 38537; doi: 10.1038/srep38537 (2016).

Publisher's note: Springer Nature remains neutral with regard to jurisdictional claims in published maps and institutional affiliations.



This work is licensed under a Creative Commons Attribution 4.0 International License. The images or other third party material in this article are included in the article's Creative Commons license, unless indicated otherwise in the credit line; if the material is not included under the Creative Commons license, users will need to obtain permission from the license holder to reproduce the material. To view a copy of this license, visit <http://creativecommons.org/licenses/by/4.0/>

© The Author(s) 2016

Supplementary Material

Self-patterning Gd nano-fibers in Mg-Gd alloys

Yangxin Li ^{1,2}, Jian Wang ³, Kaiguo Chen ⁴, Meiyue Shao ², Yao Shen ^{1*}, Li Jin ^{2*}, Guozhen Zhu ^{1*}

¹State Key Laboratory of Metal Matrix Composites, ²National Engineering Research Center of Light Alloy Net Forming, School of Materials Science and Engineering, Shanghai Jiao Tong University, 800 Dongchuan Rd., Shanghai 200240, P.R. China.

³Department of Mechanical and Materials Engineering, University of Nebraska-Lincoln, Lincoln, NE, 68588, USA.

⁴National Key Lab of Shockwave and Detonation Physics, Institute of Fluid Physics, China Academy of Engineering Physics, Mianyang, Sichuan 621000, P.R. China.

¹ Correspondence and requests for materials should be addressed to Y.S. (Email: yaoshen@sjtu.edu.cn), L.J. (Email: j_jinli@sjtu.edu.cn), or G.-z. Z. (zhugz@sjtu.edu.cn).

Experimental Methods:

1. Experimental alloys

Mg-1Gd (wt.%) alloy billets, with 60 mm in diameter and 50 mm in length, were prepared through melting high purity Mg (99.99%) and Mg-25wt.%Gd master alloys in an electric furnace under a protective gas mixture of SF₆/CO₂. The billets were partly indirect extruded at temperatures of 400°C with extrusion ratio of 16. The billets were heated to the extrusion temperature and held isothermally for 30 mins before extrusion. Extrusion experiments were stopped when the billets had been extruded to 150 mm from the die, and the die and butt were removed from the machine and quenched together into a water bath. As the extrusion butt was quenched immediately after extrusion, static recrystallization was hindered and the dynamically recrystallized microstructure during extrusion was preserved. After extrusion, samples were isochronally annealed at 200°C, 250°C, 300°C for 2-4 hours.

2. Sample preparation and TEM characterization

The as-fabricated Gd-Mg alloys were cut into slices with ~600 μm in thickness, and then mechanically ground to ~100 μm. TEM discs with 3 mm in diameter were punched out from the slices, and then twin-jet electro-polished in an ethanol solution with 4 pct perchloric acid. TEM specimens were further thinned at 500 eV for 0.5 h using Gatan precision ion polishing system (PIPS II MODEL 695). Structural characterization was carried out under scanning transmission electron microscopy (STEM) mode at 200 kV using a JEOL-ARM200F microscope with a

probe-forming lens corrector. Due to the large difference in atomic numbers of Gd and Mg, high-angle annular dark-field (HAADF) imaging technique was applied to image Gd atoms in binary Mg-Gd alloys. The probe convergence semi-angle was approximately 30 mrad. The collection semi-angle of the annular dark-field (ADF) detector was ~68-280 mrad.

Supplementary Text:

1. Distribution of the hexagonal patterns

Viewed along [0001], Figure S1 shows a typical grain of a few microns in size. Since hot extrusion was carried out at 400°C and cooled down immediately, no twins were detected in as-extruded samples and those with 200°C and 250°C annealing. Even in the as-extruded sample in Figure S1, we did not find a high density of dislocations, except some grains with dislocation pile-up near their grain boundaries. At grain boundaries, Gd segregation with short-range ordering was clearly observed, which is consistent with the previous report.⁽¹⁾ Within most grains, we detected a huge number of low-angle grain boundaries, consisting of segregated dislocations. Some of these low-angle grain boundaries accompanies with hexagonal patterns, labeled as the red arrows in Figure S1a. Those hexagonal patterns are less than 200 nm in width and a few microns in length. The interspacing within those hexagonal patterns is usually in the range of 3-20 nm, with a predominant interspacing of ~10 nm.

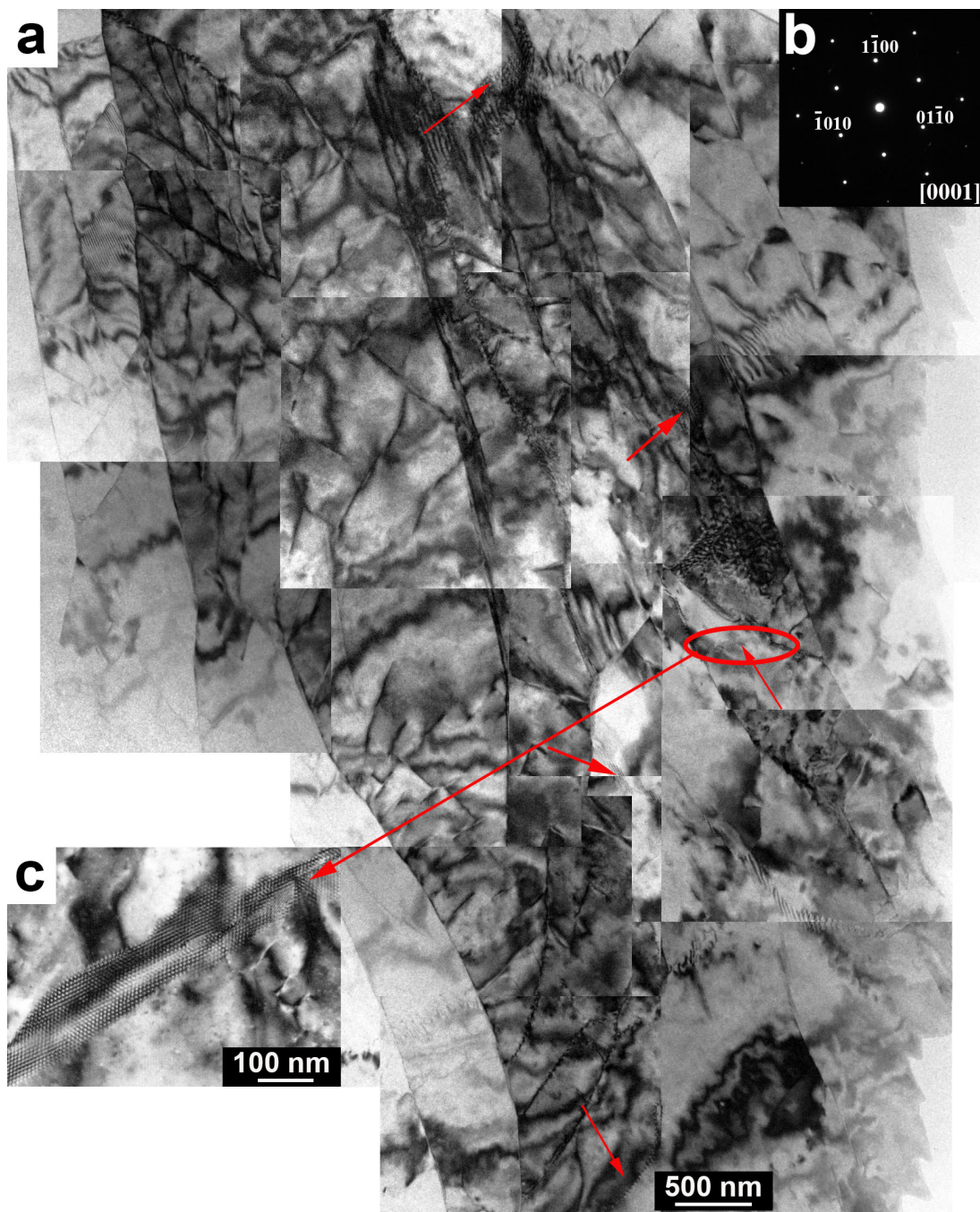


Figure S1. TEM images showing the distribution of hexagonal patterns in one grain viewed along the [0001], as indicated from the diffraction pattern in **b**. **c**, An enlargement of the elliptical area in **a**. Such hexagonal patterns, with <200nm in width and ~ micron in length, are always connected with low-angle grain boundaries.

2. Low-angle grain boundaries with Gd-segregated dislocations

When the electron beam is along $\langle 0001 \rangle$, low-angle grain boundaries consist with a set of Gd-segregated dislocations, showing as the array of bright dots in the HAADF images in Figure S2. Most low-angle grain boundaries detected are along $\langle 1\bar{1}00 \rangle$. The associated dislocations have the identified Burgers vector of $\frac{1}{3}\langle 11\bar{2}0 \rangle$. The identified Burgers vectors can change their crystallographic directions, e.g. with 60° rotation, corresponding to the steps and kinks at the low-angle grain boundaries. Some low-angle grain boundaries are along $\langle 11\bar{2}0 \rangle$, with alternating dislocations of identified Burgers vector $\frac{1}{3}\langle 11\bar{2}0 \rangle$. It should be noted that we couldn't identify the Burgers vector for a few low-angle grain boundaries, because the dislocations in these boundaries show a pure $\langle c \rangle$ component, parallel to the beam direction. As shown in the red arrows in Figure S2, the hexagonal patterns of Gd segregation were found to form along low-angle grain boundaries. In addition, the hexagonal patterns are preferentially located beside Gd-segregated dislocations changing their Burgers vector directions.

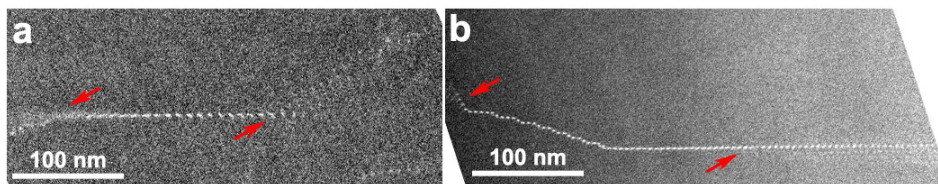


Figure S2. STEM-HAADF raw images of Gd-segregated arrays. The low-angle grain boundaries were always found at the start or end of these Gd segregated arrays. Most low-angle grain boundaries are along $\langle 1\bar{1}00 \rangle$ and those arrays preferentially start with the dislocations changing their identified Burgers vectors (also see Figure 2).

3. Burgers vector with c-components

The types of dislocations were identified under different two-beam conditions, $g = 0002$ and $g = 10\bar{1}0$, respectively. The invisible dislocations in Figure S3b with diffraction vector of $g = 10\bar{1}0$, have Burgers vectors with $\langle c \rangle$ -component. It should be noted that cross-slip trails were observed, suggesting the activation of $\langle c \rangle$ slips. The existence of Burgers vectors $\langle 0001 \rangle$ and the activation of $\langle c \rangle$ slips are required to form the hexagonal patterns.

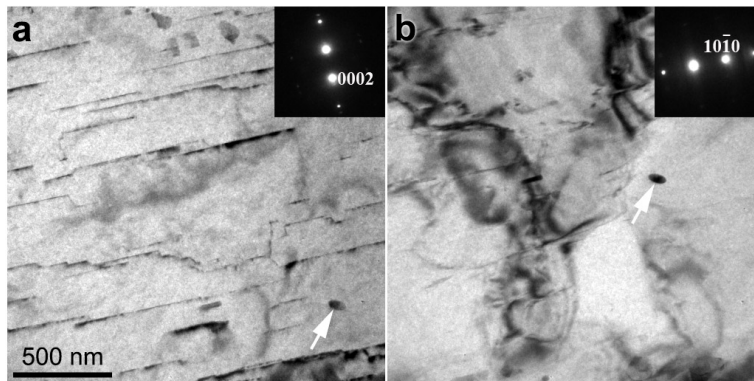


Figure S3. TEM-BF images under two-beam conditions with diffraction vector of $g=0002$ (**a**) and $g=10\bar{1}0$ (**b**), respectively. The dislocation with $\langle c \rangle$ -components is confirmed. The white arrows labeled the same area in **a** and **b**.

4. Gd-segregation viewed from $\langle 1\bar{1}00 \rangle$

Figure S4 shows the hexagonal patterns when the electron beam is along $\langle 1\bar{1}00 \rangle$. These Gd-nano-fibers are along $\langle 0001 \rangle$. As shown in Figure S4b, the interspacing between the segregated lines is approximately 5 nm.

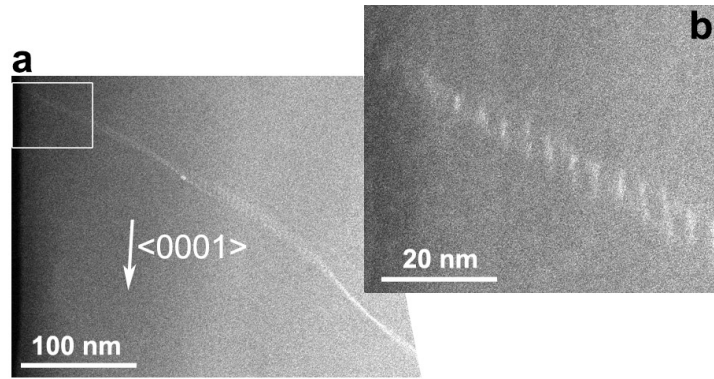


Figure S4. STEM-HAADF raw images showing Gd nano-fibers viewed from $\langle 1\bar{1}00 \rangle$. **b**, Enlarged view of the boxed region labeled in **a**.

5. Hexagonal pattern with large interspacing

Viewed along $\langle 0001 \rangle$, some hexagonal patterns have a large interspacing, e.g. 20 nm, compared to the typical value of 10 nm. (See Figure S5a). As shown in Figure S5b and c with enhanced contrast after Fast Fourier Transform (FFT) filtering, those hexagonal patterns include barely visible Gd-segregations with a cellular structure. Due to its weak contrast, it is hard to locate the template, the low-angle grain boundary with 20 nm interspacing between dislocations.

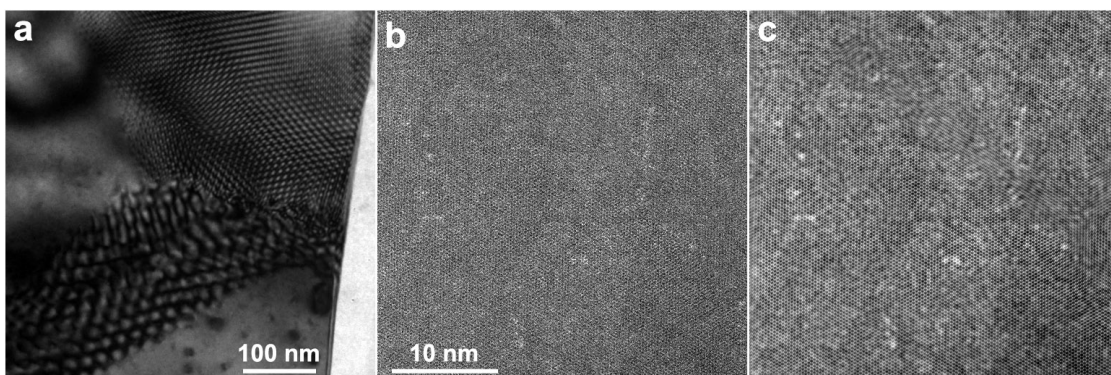


Figure S5. The hexagonal pattern showing in TEM-BF images in **a** with interspacing of ~ 20 nm. **b**, The STEM-HAADF raw images of hexagonal pattern with ~ 20 nm interspacing. **c**, The FFT filtered image of **b**.

6. Hexagonal pattern in as-excluded samples

As shown in Fig S6, hexagonal patterns are under developed in as-excluded samples. Viewed along $\langle 0001 \rangle$, Burgers vectors of $\frac{1}{3}\langle 11\bar{2}0 \rangle$ were identified at some Gd-segregations. The cellular structure has relatively weak contrast because Gd solutes have not been fully segregated into dislocations.

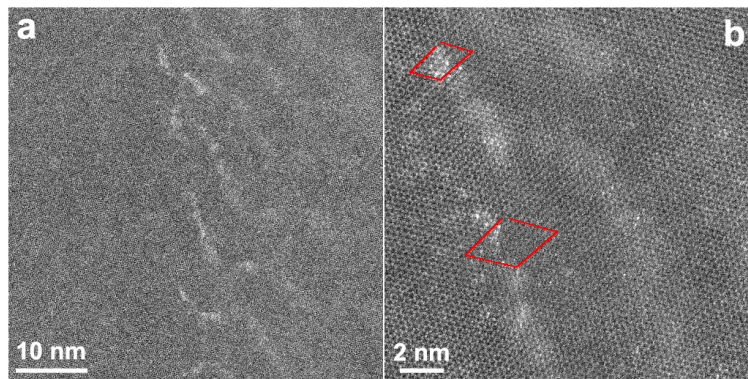


Figure S6. STEM-HAADF raw images of as-excluded sample indicating the evolution of Gd segregated arrays. **b**, Enlarged view of **a**.

7. Microstructure after 300°C annealing

Gd-segregations and their hexagonal patterns form right after hot extrusion, have better shape after 200°C and 250°C annealing, and can be destroyed at higher temperature. Within samples after 300°C annealing (see TEM images in Fig. S7), annealing twins, instead of hexagonal patterns, were recorded. We did not find twins in as-extruded samples and annealed samples at 200°C and 250°C. The existence of annealing twins is consistent with the fact that Mg alloys has a recrystallization temperature of ~260°C (15).

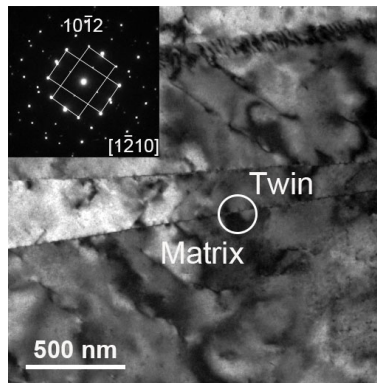


Figure S7. TEM-BF images of annealed sample at 300°C for 4 hours, showing the formation of an annealing twin.

8. Hexagonal pattern of dislocations

Figure S8 is schematics of the dislocation components in the patterned fibers. The columns other than the one forming the low-angle grain boundary are composed of screw dislocations of alternative signs, and the grain boundary dislocations are of $\langle a+c \rangle$ dislocations, with the signs of $\langle a \rangle$ edge dislocations identical but those of the $\langle c \rangle$ screw dislocations alternating. Such a picture comes up with several facts: (1) There is no contribution of misorientation across these fibers from these non-grain boundary dislocations, as the misorientation of the parts outside of the

fibers are the same of that produced by the single column of low-angle grain boundary dislocations; (2) The diffraction pattern of the local area is very sharp indicating a sharp, rather than gradual, transition of orientations; (3) There is no interactions between screw dislocations and edge dislocations since it is isotropic in the basal plane of a hexagonal lattice and isotropic theory works exactly for dislocations parallel to the $\langle c \rangle$ -axis; (4) Gd fibers are formed by segregation to dislocation cores.

Stability of such patterns is evaluated by checking the maximum resolved stress on each slip system of the non-grain-boundary screw dislocations. The grain boundary are stabilized by its edge components and its screw components are thus anchored to the edge ones. Simple calculations show that when the number of dislocations in the column is larger than the order of 10, the maximum resolved stress on a screw dislocation from all other dislocation in the pattern are below $4 \times 10^{-3} \mu$ except for the one or two dislocations at each end. These columns can be stabilized since the Peiers stress of the dislocations, the minimum stress needed to move a straight dislocation, is well above $4 \times 10^{-3} \mu$ for the dislocations in the prismatic planes with the pinning effect of Gd solution (16-17). The dislocations at each end can be stabilized by other defects such as grain boundary or threading dislocations.

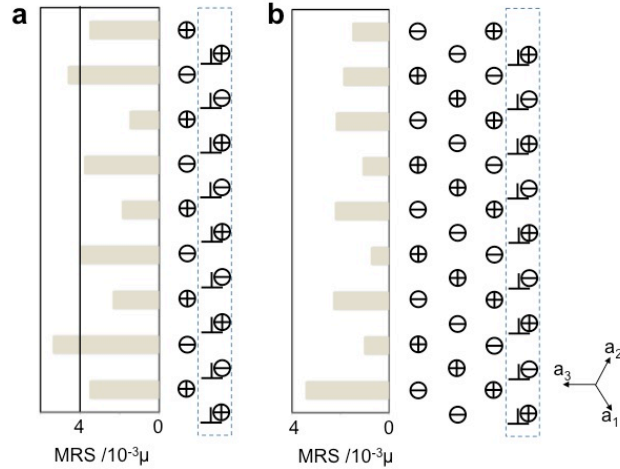


Figure S8. Schematics of the dislocations patterns. **a**, A pattern of two columns, **b**, A pattern of multiple (four) columns. The low-angle grain boundaries are composed of mixed $\langle c+a \rangle$ dislocations, while other columns are of screw ($\langle c \rangle$, in circles) dislocations. A circle with “+” inside denotes a positive screw dislocation, while one with “-” inside a negative screw dislocation. a_1 , a_2 and a_3 show the $\langle 11\bar{2}0 \rangle$ directions in the basal plane. The bar-figures show the maximum resolved stress (MRS) of the left or left-most column on one of the three $\langle a \rangle$ slip systems.

8. Tensile Responses

Due to these difficulties in quantifying the volume ratio of Gd-fiber patterns, we cannot quantify the Gd fiber-reinforced effect on the mechanical properties. A few tensile tests indicate the positive effect caused by the Gd-fiber pattern. In order to maintain the identified texture caused from hot extrusion, we compared the tensile results of extruded samples and indirect-extruded samples. The indirect-extruded samples, with the embryo of Gd-fiber patterns, have at least 20% strengthen effect compared to the normally extruded samples, which have no Gd-fiber pattern.

The normally extruded samples experience additional annealing treatment associated to the normal extrusion processes, which destroys any possible Gd-fiber pattern. In addition, we performed the tensile tests for indirect-extruded samples, with Gd-fiber patterns after additional aging at 200°C. As shown in Figure S9, the self-patterning Gd-fibers do slightly increase both the strength and ductility even after intermediate annealing treatment.

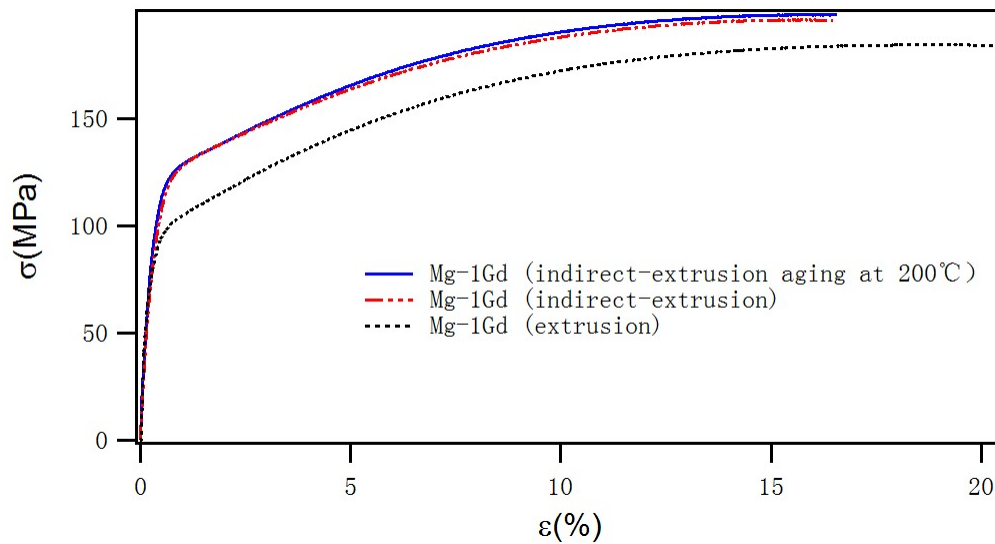


Figure S9. Tensile results of Mg-Gd alloys with/without Gd nano-fiber patterns. The black, red and blue curves present the mechanical responses of Mg-Gd alloys without any patterns, with the embryo, and with the Gd-fiber patterns, respectively.

References

1. Bugnet, M. et al. Segregation and clustering of solutes at grain boundaries in Mg-rare earth solid solutions. *Acta Mater.* 79, 66–93 (2014).